Materials Today Bio 28 (2024) 101202

Contents lists available at ScienceDirect

Materials Today Bio

journal homepage: www.journals.elsevier.com/materials-today-bio

Therapeutic framework nucleic acid complexes targeting oxidative stress and pyroptosis for the treatment of osteoarthritis

Jiafeng Li [a,1], Yifan Li [a,1], Xiushuai Shang [a,1], Sheng Xu [b], Zhen Zhang [a], Sanzhong Xu [a,*], Xuanwei Wang [a,**], Miaoda Shen [a,***]

[a] Department of Orthopedics, The First Affiliated Hospital, Zhejiang University School of Medicine, No. 79 Qingchun Road, Hangzhou, China
[b] Department of Orthopedics, People's Hospital of Changshan County, Quzhou, China

ARTICLE INFO

Keywords:
Tetrahedral framework nucleic acids
Nobiletin
Osteoarthritis
Oxidative stress
Pyroptosis

ABSTRACT

Osteoarthritis (OA) is one of the most prevalent joint diseases and severely affects the quality of life in the elderly population. However, there are currently no effective prevention or treatment options for OA. Oxidative stress and pyroptosis play significant roles in the development and progression of OA. To address this issue, we have developed a novel therapeutic approach for OA that targets oxidative stress and pyroptosis. We synthesized tetrahedral framework nucleic acid (tFNAs) to form framework nucleic acid complexes (TNCs), which facilitate the delivery of the naturally occurring polymethoxyflavonoid nobiletin (Nob) to chondrocytes. TNC has demonstrated favorable bioavailability, stability, and biosafety for delivering Nob. Both *in vitro* and *in vivo* experiments have shown that TNC can alleviate OA and protect articular cartilage from damage by eliminating oxidative stress, inhibiting pyroptosis, and restoring the extracellular matrix anabolic metabolism of chondrocytes. These findings suggest that TNC has significant potential in the treatment of OA and cartilage injury.

1. Introduction

Osteoarthritis (OA) is a highly prevalent joint disease that significantly impacts the quality of life in the elderly population [1,2]. OA is characterized by articular cartilage degeneration, subchondral bone sclerosis, osteophyte formation, and chronic synovitis, clinically presenting as gradually progressive pain, stiffness, and functional impairment in the joints [3,4]. The prevalence of OA remains substantial, exerting a significant impact on quality of life and imposing considerable socioeconomic burdens globally [5]. Currently, there is a lack of effective preventive measures or treatments for OA, with drug therapy and joint replacement being the only options available in advanced stages of the disease [6,7]. The pathogenesis of OA encompasses a multitude of factors, wherein the degradation of the extracellular matrix (ECM) leading to articular cartilage degeneration emerges as one of the pivotal determinants [8,9]. Under physiological conditions, chondrocytes play a crucial role in maintaining the homeostasis of the ECM and preserving the structural integrity of articular cartilage through a delicate balance between matrix synthesis and degradation [10]. However, in the pathogenesis of OA, disruption of this delicate equilibrium can result in excessive chondrocyte damage and ECM degeneration, ultimately exacerbating articular cartilage degeneration. In the early stages of OA development, stimulation by inflammatory cytokines can induce chondrocytes to excessively produce matrix-degrading enzymes, thereby disrupting ECM homeostasis and accelerating articular cartilage degeneration [11,12].

Oxidative stress and pyroptosis can disrupt the homeostatic balance of chondrocytes, leading to cartilage damage and the pathogenesis of OA [13,14]. The accumulation of reactive oxygen species (ROS) and a concurrent decrease in antioxidant defenses result in heightened oxidative stress, which subsequently activates numerous catabolic mediators and accelerates the degradation of the cartilage ECM [15]. In addition, previous clinical studies have demonstrated an interrelation between oxidative stress, aging, and OA [16]. In OA chondrocytes,

* Corresponding author. Department of Orthopedics, The First Affiliated Hospital, Zhejiang University School of Medicine, No. 79 Qingchun Road, Hangzhou, 310003, China.
** Corresponding author.
*** Corresponding author.
E-mail addresses: xusanzhong@zju.edu.cn (S. Xu), 1507130@zju.edu.cn (X. Wang), mds@zju.edu.cn (M. Shen).
[1] Contributed equally.

https://doi.org/10.1016/j.mtbio.2024.101202
Received 7 June 2024; Received in revised form 3 August 2024; Accepted 12 August 2024
Available online 20 August 2024

ROS-induced oxidative damage induces cellular senescence that impairs chondrocyte proliferation and viability [13].

Previous studies have demonstrated that the activation of the NLRP3 inflammasome induces pyroptosis through oxidative stress [17]. An increasing body of evidence suggests that pyroptosis plays a significant role in the pathogenesis and progression of OA [14,18,19]. Pyroptosis is a recently identified form of programmed cell death characterized by inflammatory responses and cellular demise [20]. Inflammasomes are protein complexes comprising NOD-like receptor family pyrin domain containing 3 (NLRP3), apoptosis-associated speck-like protein (ASC), and Caspase-1 (CASP1) [21]. Upon activation of the inflammasome, Caspase-1 is triggered, leading to the maturation and subsequent release of IL-1β and IL-18, as well as the proteolytic cleavage of gasdermin D (GSDMD) [22]. In OA chondrocytes, the activation of pyroptosis can be induced by oxidized low-density lipoprotein (OxLDL) and lipopolysaccharide (LPS) [23,24]. The occurrence of pyroptosis in articular cartilage disrupts the metabolic homeostasis of chondrocytes, ultimately contributing to the cartilage degeneration and OA onset [25]. Therefore, targeting the elimination of ROS, alleviating oxidative stress, and inhibiting pyroptosis represent pivotal strategies for the therapeutic management of OA.

Emerging research underscores the significance of small molecule drugs in the treatment of OA, where they exert therapeutic effects through their antioxidant and antipyroptotic properties [26,27]. Nobiletin (Nob) is a naturally occurring polymethoxyflavone compound derived from the peels of citrus fruits [28]. Due to its broad spectrum of pharmacological effects, which include antioxidant [29], anti-inflammatory [30], and antipyroptotic activities [31], Nob has demonstrated potential therapeutic efficacy against a variety of diseases, including cancer and OA. Research has revealed that Nob in both IL-1β-induced human OA chondrocytes and surgical destabilization of the medial meniscus (DMM) mouse models of OA, IL-1β has been shown to exert anti-inflammatory and protective effects on chondrocytes by inhibiting the phosphatidylinositol-4,5-bisphosphate 3-kinase/protein kinase B (PI3K/Akt) and nuclear factor kappa B (NF-κB) pathways, demonstrating its potential value in the treatment of OA [32]. Additionally, Nob has been shown to mitigate oxidative stress, restore mitochondrial membrane potential, and inhibit the expression of MMP3 and MMP13, potentially improving the symptoms of rheumatoid arthritis (RA) [33]. Considering the rapid metabolism and relatively poor aqueous solubility of Nob within the joint cavity, a sophisticated drug delivery system is crucial for the sustained therapeutic effect of Nob on OA.

Tetrahedral framework nucleic acids (tFNAs) represent a novel class of DNA nanomaterials capable of self-assembling into tetrahedral structures through the temperature-dependent interaction of four single-stranded DNA molecules [34,35]. tFNA exhibit excellent biocompatibility, safety, programmability, and mechanical stability, which are highly desirable attributes for a variety of biomedical applications [36–38]. In chondrocytes stimulated by IL-1β, tFNA has been demonstrated to effectively suppress oxidative stress and apoptosis, thereby serving a protective role for cartilage and exhibiting potential in the alleviation of OA [39]. Previous studies have demonstrated the successful delivery of microRNAs (miRNAs), small molecule drugs, and peptides to chondrocytes using tFNA for the treatment of OA [35, 40–42].

In the present study, we constructed a novel nanoparticle, TNC, which is a tFNA/Nob complex formed by loading Nob onto tFNA and serves as an efficient drug delivery system for Nob. We hypothesized that these novel nanoparticles may play a role in alleviating oxidative stress and pyroptosis, as well as promoting ECM anabolism, in the treatment of OA. Furthermore, we utilized tert-butyl hydroperoxide (TBHP) to stimulate chondrocytes and established a destabilization of the medial meniscus (DMM) animal model to validate the therapeutic effects of TNC in both *in vitro* and *in vivo* models.

2. Results and discussion

2.1. Preparation and characterization of tFNA and TNC

Based on the principle of base pairing, tFNAs were assembled using four single-stranded DNA molecules (Table 1) [35]. Four DNA strands were connected end-to-end to form a stable tetrahedral structure. Subsequently, Nob was combined with tFNA through oscillation to form a TNC complex (Fig. 1A). The molecular structure of Nob is shown in Fig. 1D. Previous studies have shown that flavonoids can directly interact with DNA by embedding into the double-stranded DNA and preferentially binding to the DNA structure [43]. The morphology of TNC was characterized by AFM and TEM (Fig. 1B and C). As shown in Fig. 1E, the UV–visible absorption spectrum of natural Nob in DMSO solution was revealed by scanning, showing a prominent high absorption peak at around 340 nm. The high absorption peak of tFNA was located at around 260 nm. TNC showed two absorption peaks, with the value at around 340 nm being close to the absorption peak value of natural Nob, confirming the successful encapsulation of Nob in tFNA. Then, the AGE result (Fig. 1F) was obtained to verify the synthesis of the materials. This indicates that the tFNA were successfully synthesized and are not affected by Nob. Furthermore, the visible difference between synthetic TNC and free Nob is shown in Fig. 1G. TNC appears as a clear, transparent liquid, while free Nob is observed as an insoluble Nob in PBS. This confirms that TNC disperses well in aqueous solution. To determine the encapsulation efficiency of TFNs carrying Nob, we measured the encapsulation efficiency of different fractions of components as shown in Fig. S1. Based on previous experiments, the concentration of tFNA was fixed at 250 nM [35,44]. The results showed that the encapsulation efficiency of Nob loaded onto TFNA decreased, and the relative optimal encapsulation efficiency was achieved when 40 μM Nob was loaded onto 250 nM tFNA. It is worth noting that the encapsulation rate of 40 μM Nob to 250 nM tFNA was significantly better than that of other components. Therefore, in subsequent experiments, we chose to use 40 μM Nob and 250 nM tFNA to synthesize TNC. We employed dynamic light scattering (DLS) to analyze the particle size and zeta potential of the tFNA and TNC. As illustrated in Fig. 1H, the size and zeta potential of the tFNAs were 10.21 ± 3.42 nm, and the zeta potential was -5.31 ± 1.24 mV. For TNC, the corresponding particle size was 35.42 ± 2.54 nm, and the zeta potential was -16.42 ± 4.25 mV. TNC exhibits a more negative zeta potential and a larger size. According to the DLVO theory [40], TNC possesses greater structural stability. Subsequently, we evaluated the sustained release of Nob from TNC. As depicted in Fig. S2, within a period of 36 h, TNC gradually released Nob, with the release ratio remaining below 50 %. After 36 h, there was a significant increase in the release rate, reaching nearly 100 % by 72 h. The sustained release of Nob by TNC is crucial for the effective treatment of OA. Subsequently, we evaluated the serum stability of TNC/tFNA. The results obtained from the AGE assay in Fig. 1I demonstrate that free tFNA undergoes nearly complete degradation after approximately 10 h in both 2 % and 10 % fetal bovine serum (FBS). In contrast, TNC exhibited degradation at around 12 h. These findings suggest that TNC possesses biostability comparable to that of tFNA, with additionally benefiting from enhanced stability conferred by the complexation between TNC and tFNA. We employed Cy5 fluorescence labeling of single-stranded nucleic acids and confocal microscopy to investigate the cellular uptake of tFNA and TNC. Immunofluorescence (IF) images (Fig. 1J and K) demonstrated that the cellular uptake of TNC surpassed that of tFNA at both 6 and 12 h, further substantiating the exceptional delivery capability of TNC.

Due to the poor water solubility of Nob, its bioavailability and plasma stability are limited. Consequently, various nanodelivery systems have been developed for loading Nob. Qu et al. utilized a self-nanoemulsifying drug delivery system (SNEDDS) to deliver TGPs and P-glycoprotein (P-gp) inhibitor Nob effectively for treating refractory arthritis in rats with rheumatoid arthritis [45]. Ning et al. employed Soluplus and PVP/VA 64 as carriers to prepare a novel self-assembled

Table 1
Sequence of four ssDNA.

ssDNA	Direction	Base sequence
S1	5′ to 3′	ATTTATCACCCGCCATAGTAGACGTATCACCAGGCAGTTGAGACGAACAT TCCTAAGTCTGAA
S2	5′ to 3′	ACATGCGAGGGTCCAATACCGACGATTACAGCTTGCTACACGATTCAGAC TTAGGAATGTTCG
S3	5′ to 3′	ACTACTATGGCGGGTGATAAAACGTGTAGCAAGCTGTAATCGACGGGAAG AGCATGCCCATCC
S4	5′ to 3′	ACGGTATTGGACCCTCGCATGACTCAACTGCCTGGTGATACGAGGATGGG CATGCTCTTCCCG
Cy5-S1	5′ to 3′	Cy5-ATTTATCACCCGCCATAGTAGACGTATCACCAGGCAGTT GAGACGAACATTCCTAAGTCTGAA

nanomedicine delivery system using thermo-melting extrusion technology, which enhanced the liver protective effect of Nob on acetaminophen (APAP)-induced acute liver injury (AILI) [46]. Wu et al. designed a biocompatible and biodegradable film based on metal-phenol coordination chemistry for encapsulating Nob, achieving controlled drug release *in vitro* and *in vivo* to enhance its bioactivity and bioavailability in cancer therapy [47]. Wang et al. synthesized NOB-polyethylene glycol-polycaprolactone block copolymers by dialysis, effectively preventing bone loss in OVX mice and improving bone density [48]. Similarly, TNC has successfully addressed the challenges of low bioavailability and instability of Nob in physiological fluids, showing great potential for application in OA treatment.

2.2. TNC alleviated TBHP-induced oxidative stress in C28/I2 cells

The accumulation of ROS induce oxidative stress, leading to chondrocyte damage and senescence, ultimately resulting in cartilage degeneration [49]. Therefore, the inhibition of oxidative stress is crucial for maintaining ECM metabolism. Based on previous research findings, both free tFNA and Nob have demonstrated effective ROS scavenging and antioxidant capabilities [28,50]. We subsequently evaluated the *in vitro* antioxidant stress capabilities of Nob, tFNA, and TNC. In our initial evaluation, we employed the DCFH-DA probe to quantify intracellular ROS levels. We initially established an oxidative stress injury model in C28/I2 cells by stimulating them with TBHP (100 μM), a well-known inducer of oxidative stress. The stimulatory effects of TBHP on both oxidative stress and pyroptosis of chondrocytes have been previously confirmed [51,52]. As illustrated in Fig. 2A, treatment with TBHP significantly augmented ROS production, indicating successful establishment of the oxidative stress model. Subsequently, both Nob (40 μM) and free tFNA (250 nM) treatments effectively attenuated ROS levels, demonstrating robust anti-ROS effects consistent with previous findings. Notably, TNC exhibited the most potent ability to scavenge ROS, effectively reducing ROS levels to a level comparable to that of normal cells. Oxidative stress is known to induce mitochondrial membrane potential depolarization [53]. Therefore, we also assessed changes in mitochondrial membrane potential using the JC-1 probe. The results indicated that treatment with TBHP caused a decrease in fluorescence intensity of JC-1 aggregates and an increase in that of monomers, indicating TBHP-induced oxidative stress led to mitochondrial membrane potential depolarization (Fig. 2B and C). The mitochondrial membrane potential was significantly restored by Nob, tFNA, and TNC, with TNC exhibiting the most pronounced effect. Superoxide dismutase (SOD) is a key primary enzyme involved in antioxidant defense, while malondialdehyde (MDA) and advanced oxidation protein products (AOPPs) represent later-stage ROS products [54]. Levels of SOD, MDA, and 8-hydroxy-2′-deoxyguanosine (8-OHdG) in C28/I2 cells were quantified using corresponding assay kits. The obtained experimental results were consistent with those from the DCFH-DA and JC-1 assays, indicating that TNC had the most potent antioxidant effect against oxidative stress, followed by Nob and tFNA (Fig. 2D–F). In summary, TNC demonstrated remarkable *in vitro* ROS scavenging activity and antioxidant stress capabilities.

2.3. TNC reduced TBHP-induced cell pyroptosis in C28/I2 cells

Pyroptosis is considered as a crucial pathogenic factor contributing to the onset of OA [55,56]. In the pathogenesis of OA, stimuli such as OxLDL and LPS induce pyroptosis in chondrocytes by activating inflammasomes [23,24]. Pyroptosis induces chondrocyte death and triggers catabolic metabolism of the extracellular matrix (ECM), thereby exacerbating articular cartilage degeneration [57]. Consequently, targeting pyroptosis in chondrocytes is crucial for OA treatment. Previous research has shown that both Nob and free tFNA possess the ability to mitigate cellular pyroptosis [31,58,59]. Subsequently, the effects of Nob, tFNA, and TNC on C28/I2 cell pyroptosis were evaluated *in vitro*. Live/dead staining and CCK-8 assays showed that TBHP-induced cell viability inhibition was mediated through pyroptosis, resulting in a significant reduction in cell number. However, treatment with Nob, tFNA, or TNC alleviated this damage (Fig. 3A and B). Furthermore, Western blot (WB) analysis was performed to assess the expression of pyroptosis-associated proteins. The results demonstrated that TBHP stimulation significantly upregulated the expression of NLRP3, CASP1, and IL-1β (Fig. 3C–F). While treatment with Nob, tFNA, or TNC suppressed their expression. Notably, TNC exhibited the most pronounced inhibitory effect among all treatments. Additionally, the levels of lactate dehydrogenase (LDH) in the cell supernatant were assessed to monitor changes in pyroptosis under different treatment conditions (Fig. 3G). Consistent with the aforementioned Western blot findings, the LDH assay results supported these observations. Furthermore, CASP1 and IL-1β IFexperiments indicated that TNC demonstrated superior efficacy in mitigating pyroptosis compared to Nob and tFNA (Fig. 3H and I). In summary, TNC significantly attenuated chondrocyte pyroptosis *in vitro*.

2.4. TNC reduced TBHP-induced ECM catabolic metabolism enhancement in C28/I2 cells

Under normal physiological conditions, the equilibrium between catabolism and anabolism of the ECM in chondrocytes maintains articular cartilage homeostasis [10]. However, this balance can be disrupted by oxidative stress, pyroptosis, and apoptosis, leading to cartilage degradation and the onset of OA. Therefore, we subsequently evaluated the impact of Nob, tFNA, and TNC on ECM metabolism in C28 chondrocytes. Stimulation with TBHP resulted in reduced staining intensity of Alcian blue and toluidine blue; however, Nob, tFNA, or TNC reversed this effect. Notably, TNC exhibited the most significant effect approaching levels observed in the NC group (Fig. 4A). WB analysis revealed that TBHP stimulation led to decreased ECM anabolic metabolism as evidenced by reduced expression of type II collagen (COL2) and SRY-box 9 (SOX9) in C28/I2 chondrocyte. Conversely, catabolic metabolism marked by increased MMP3 and MMP13 was enhanced (Fig. 4B–F). However, Nob, tFNA, and TNC effectively suppressed ECM catabolism while restoring anabolic metabolism with TNC demonstrating the most pronounced effect. Previous studies have shown that Nob and tFNA can promote anabolic metabolism in chondrocytes thereby playing a protective role on cartilage matrix which is consistent with our findings [32,35]. IF for aggrecan and COL2 yielded consistent results (Fig. 4G and H). Inflammatory mediators such as prostaglandin E2 (PGE2), nitric oxide (NO), IL-6, IL-1β and tumor necrosis factor-alpha

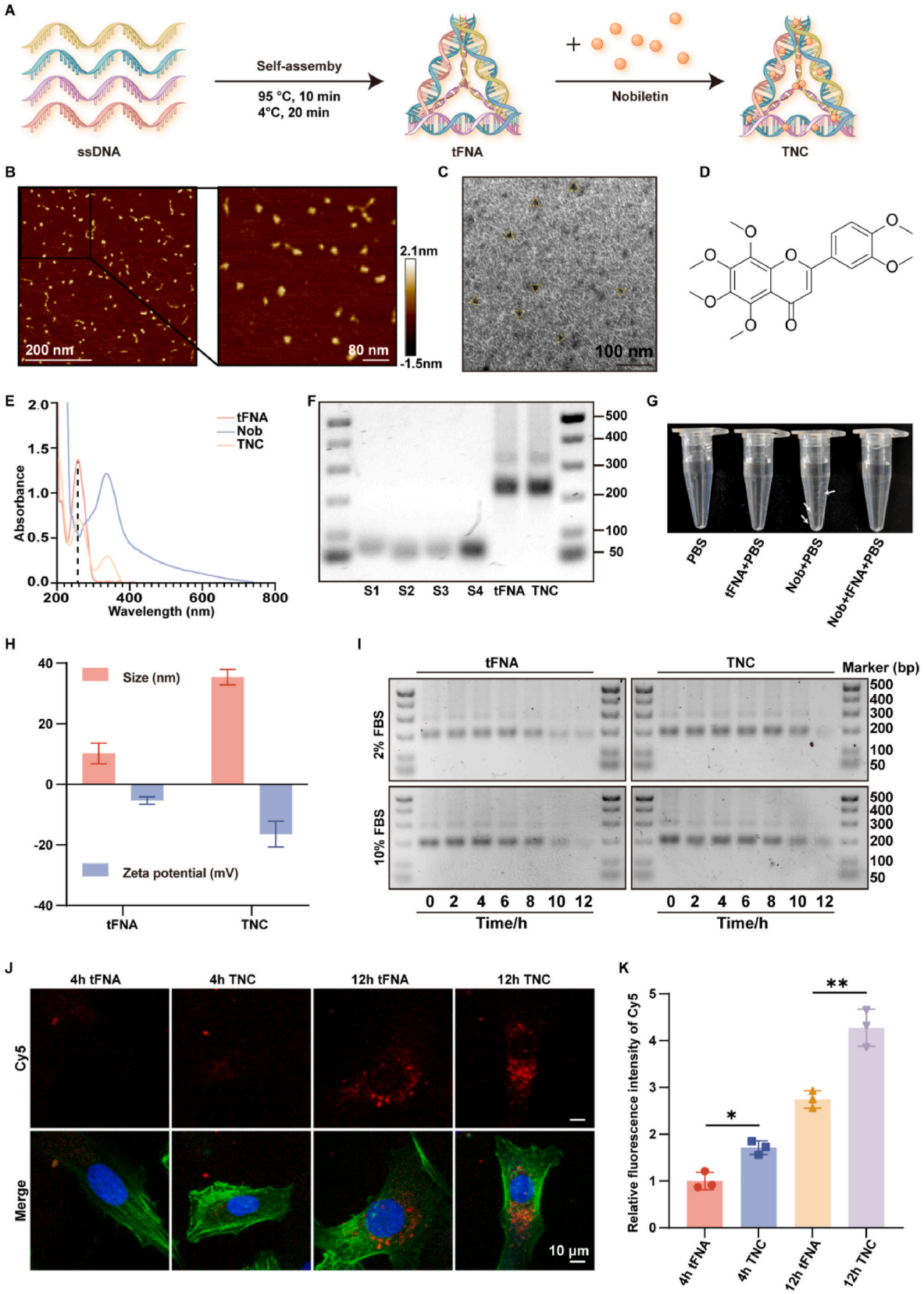

Fig. 1. Synthesis and characterization of TNC. **(A)** A schematic diagram of tFNA self-assembly and loading with the Nob component to form TNC. **(B)** the AFM image of TNC. **(C)** the TEM image of TNC. **(D)** The Molecular structure of Nob. **(E)** Spectra of Nob, tFNA and TNC between 200 and 800 nm. **(F)** Confirmation of the successful synthesis of tFNA and TNC by AGE. **(G)** Images of Nob, tFNA, and TNC dissolved in PBS solution. **(H)** the particle size and zeta potential of tFNA and TNC. **(I)** The stability of tFNA and TNC in FBS by AGE. **(J)** Cellular uptake of Cy5-tagged tFNA and TNC by C28/I2 cells was observed through immunofluorescence microscopy, where Cy5 fluorescence was depicted in red, cellular cytoskeleton in green, and nuclear staining in blue (bar = 10 μm). **(K)** Quantitative analysis of immunofluorescence results. The data are presented as the mean ± SD, n = 3.

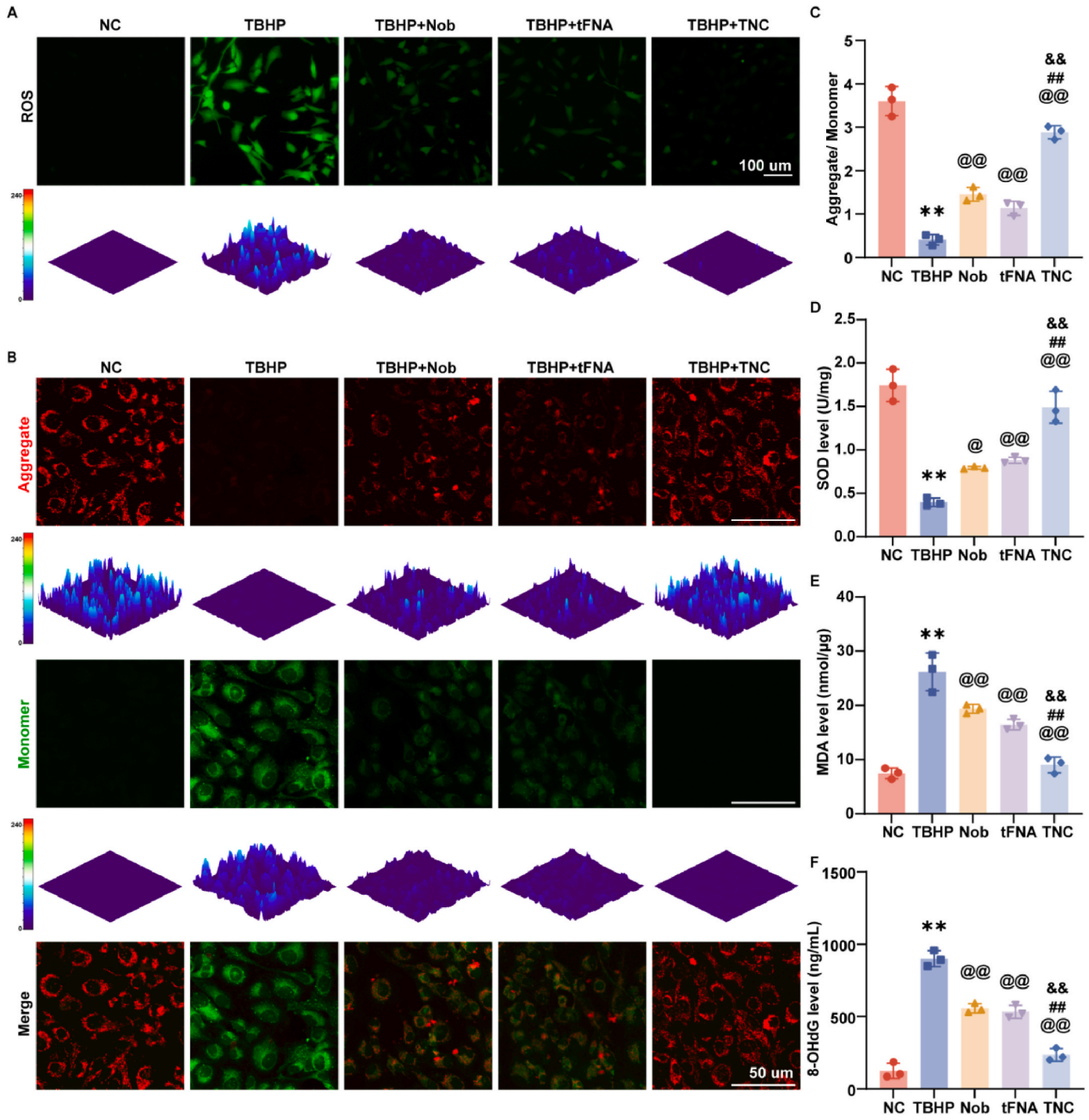

Fig. 2. TNC effectively attenuates TBHP-induced oxidative stress in C28/I2 cells. (A) Intracellular ROS levels were assessed using the DCFH-DA Probe. (B) The mitochondrial membrane potential was observed using a JC-1 probe. **(C)** The aggregate/monomer fluorescence intensity ratio of JC-1 in C28/I2 cells. **(D–F)** The levels of SOD, MDA, and 8-OHdG in C28/I2 cells were measured by corresponding assay kits. The data are presented as the mean ± SD, n = 5. *p < 0.05, **p < 0.01 relative to the NC group. $^{@}$P < 0.05, $^{@@}$P < 0.01 relative to the TBHP-stimulated group. $^{\#}$P < 0.05, $^{\#\#}$P < 0.01 relative to the Nob-treated group. $^{\&}$P < 0.05, $^{\&\&}$P < 0.01 relative to the tFNA-treated group.

(TNF-α) can enhance catabolic metabolism of chondrocytes resulting in cartilage degradation [60]. We measured inflammatory mediator levels using enzyme-linked immunosorbent assay (ELISA) kit. TBHP significantly upregulated inflammatory mediator expression in C28/I2 cells whereas TNC exhibited potent inhibitory effects on inflammation (Fig. 4I–M). In summary, TNC had a greater impact on ECM anabolic metabolism compared to Noband tFNA.

2.5. *In vivo assessment of the protective effects of Nob, TNC, and tFNA on an OA model*

Finally, the *in vivo* effects of tFNA and TNC on osteoarthritis (OA) were assessed. Mice were treated with Nob/tFNA/TNC every 2 days following DMM surgery. After 4 and 8 weeks, the mice were euthanized, and knee joints were harvested for histological examination (Fig. 5A). Initially, Safranin O, Alcian blue and Masson staining were performed to

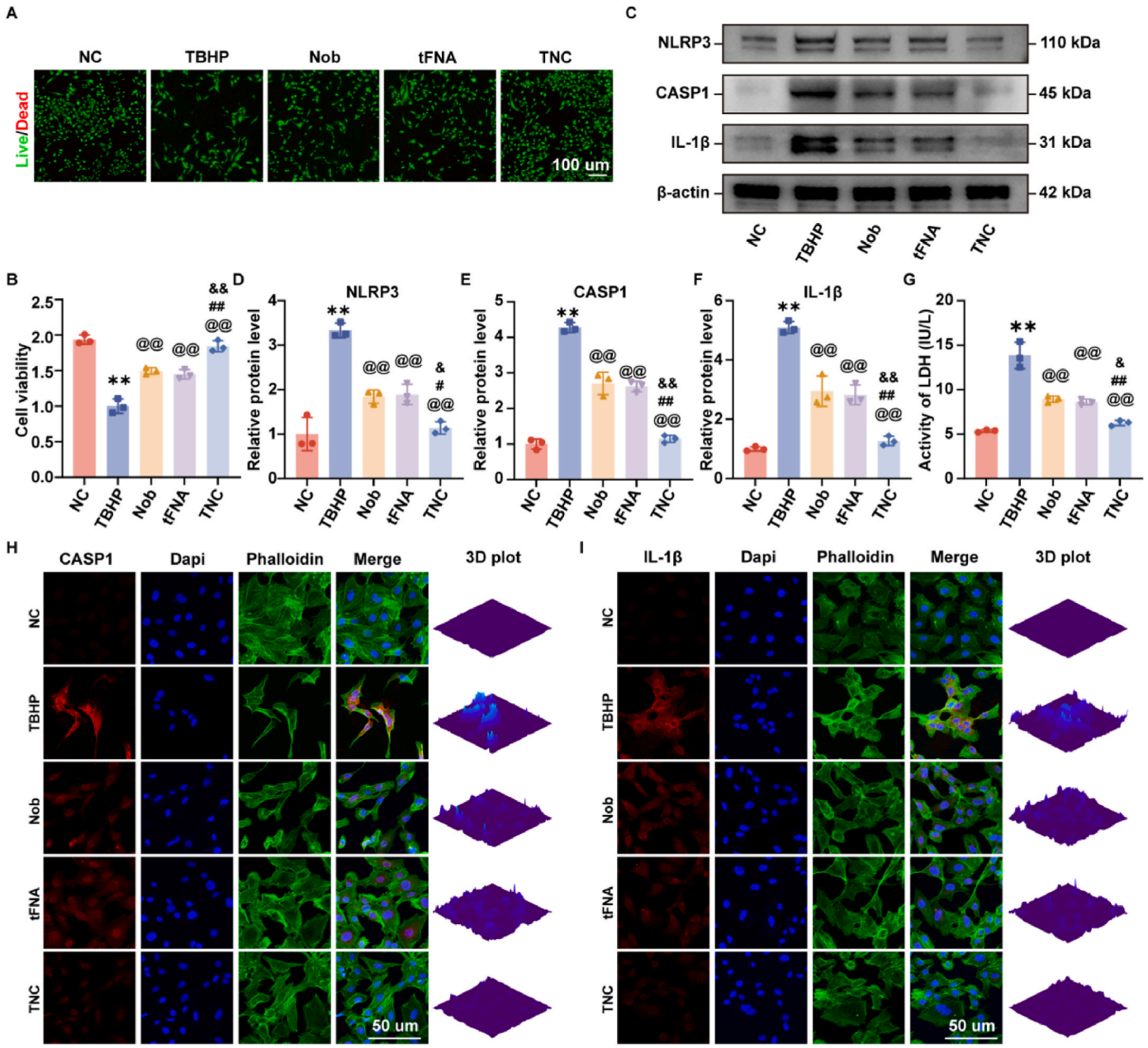

Fig. 3. TNC reduces the pyroptosis caused by TBHP in C28/I2 cells. (A, B) Live/dead staining were performed to evaluate the viability of cells, with quantitative analyze, n = 3. **(C–F)** Protein levels of CASP1, NLRP3, and IL-1β were evaluated by western blotting and statistical analysis, n = 3. **(G)** LDH activity in the supernatant of C28/I2 cells was measured using a corresponding kit. **(H, I)** IF staining of CASP1 and IL-1β in C28/I2 cells under different treatment. The data are presented as the mean ± SD. *p < 0.05, **p < 0.01 relative to the NC group. $^{@}$P < 0.05, $^{@@}$P < 0.01 relative to the TBHP-stimulated group. $^{\#}$P < 0.05, $^{\#\#}$P < 0.01 relative to the Nob-treated group. $^{\&}$P < 0.05, $^{\&\&}$P < 0.01 relative to the tFNA-treated group.

evaluate the integrity of ECM in articular cartilage. These stainings revealed severe cartilage wear and compromised integrity in the knee joints of mice after DMM surgery, confirming successful establishment of the OA animal model (Fig. 5C and Fig. S3). Furthermore, treatment with Nob and tFNA demonstrated alleviation of OA symptoms consistent with previous research [61,62]. Notably, TNC had the most pronounced effect by effectively protecting articular cartilage and reducing wear. Additionally, OARSI scoring based on Safranin O staining indicated that TNC had the most pronounced effect on alleviating OA (Fig. 5B and Fig. S4). Subsequently, IF staining was conducted for MMP13, NLRP3, and SOD2 in the knee joints to evaluate ECM metabolism oxidative stress, and cellular pyroptosis in articular cartilage. The results showed that Nob, tFNA, and TNC effectively suppressed ECM catabolism, mitigated oxidative stress, and reduced cellular pyroptosis in knee joints. TNC exhibited the most pronounced effect among them (Fig. 6A, C-E). Additionally, COL2 immunohistochemical (IHC) staining was performed on knee joints. The results confirmed findings from IF analysis where TNC group displayed highest proportion of COL2-positive cells (Fig. 6B–F). Furthermore, a WB experiment was performed using cartilage protein extracted from mouse knee joints which yielded consistent results with those obtained from IF and IHC staining (Fig. S5). The aforementioned experimental results indicate that TNC can effectively inhibit ECM catabolism, mitigate oxidative stress occurrence, and reduce cellular pyroptosis, induced by DMM in OA mice, eventually serving to protect articular cartilage and alleviate OA symptoms (Fig. 8).

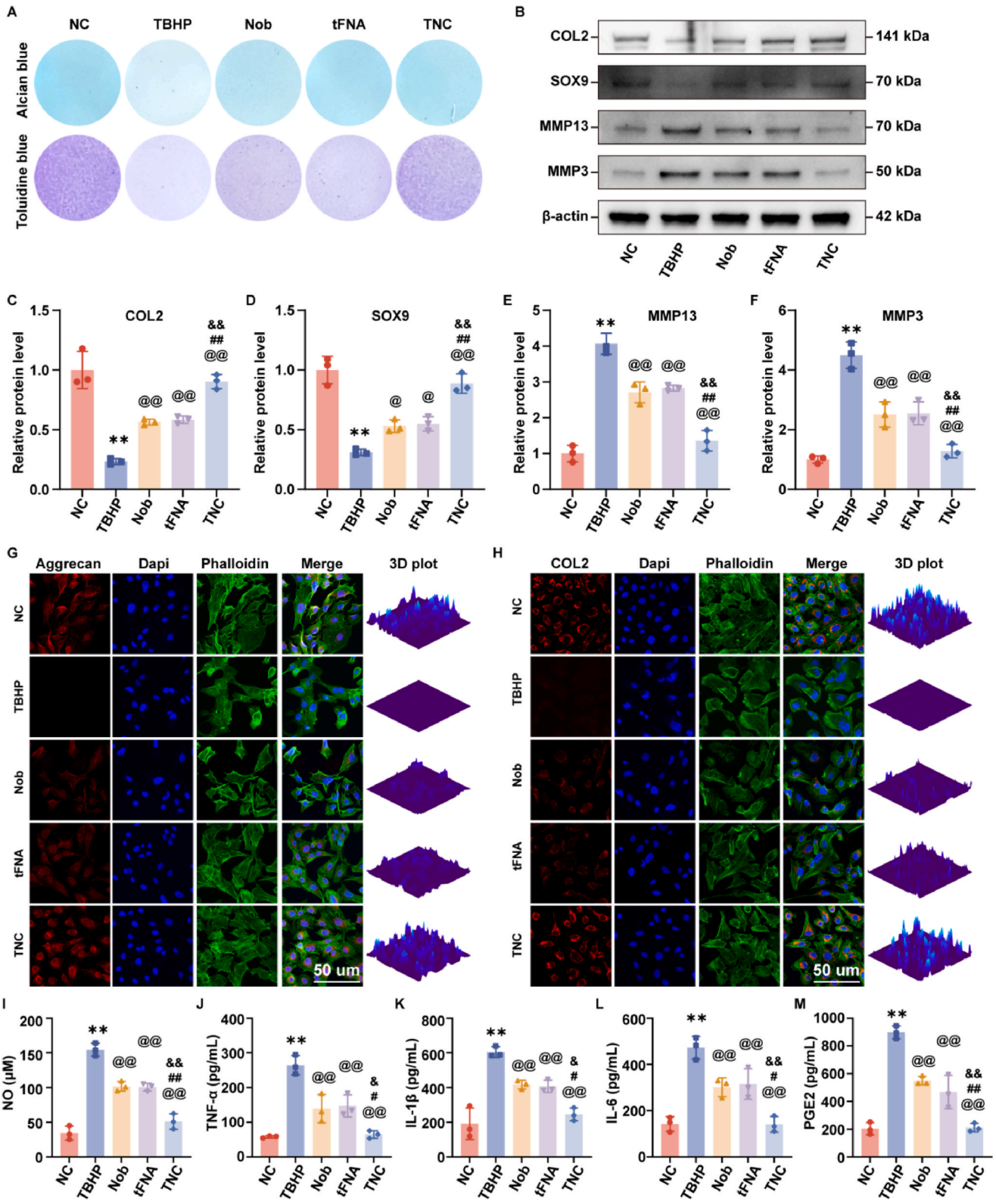

Fig. 4. The role of TNC in TBHP-induced dysregulation of extracellular matrix (ECM) metabolism in C28/I2 cells. (A) Alcian blue staining and Toluidine blue staining of C28/I2 cells. **(B–F)** Protein levels of COL2, SOX9, MMP13, and MMP3 were evaluated by western blotting and statistical analysis, n = 3. **(G, H)** IF staining of Aggrecan and COL2 in C28/I2 cells under various treatment. **(I–M)** Cytokine levels of NO, TNF-α, IL-1β, IL-6, and PGE2 were quantified in the supernatants of C28/I2 cells following various treatment, utilizing ELISA, n = 3. The data are presented as the mean ± SD, n = 3. *p < 0.05, **p < 0.01 relative to the NC group. $^{@}$P < 0.05, $^{@@}$P < 0.01 relative to the TBHP-stimulated group. $^{\#}$P < 0.05, $^{\#\#}$P < 0.01 relative to the Nob-treated group. $^{\&}$P < 0.05, $^{\&\&}$P < 0.01 relative to the tFNA-treated group.

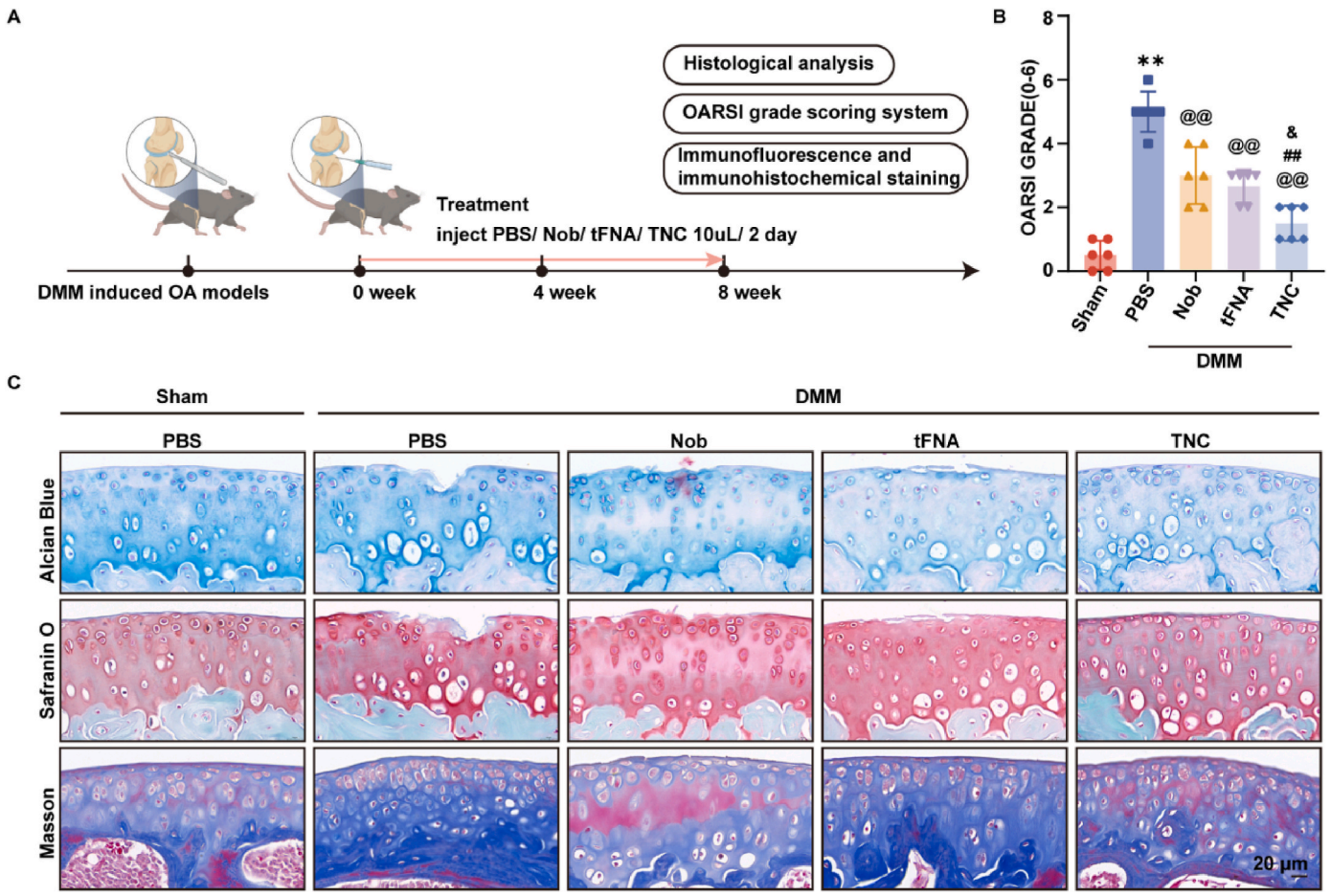

Fig. 5. ***In vivo*** **assessment of the protective effects of Nob, tFNA, and TNC on DMM OA model. (A)** Schematic diagram of Nob, tFNA, and TNC treatment for OA in DMM mice. **(B)** OARSI grade (0–6). **(C)** Images of Alcian Blue, Safranin O and Masson staining in mice knee joint articular cartilage under various treatment conditions at 8 weeks, n = 6. The data are presented as the mean ± SD. *p < 0.05, **p < 0.01 relative to the sham group. $^{@}$P < 0.05, $^{@@}$P < 0.01 relative to the DMM group. $^{\#}$P < 0.05, $^{\#\#}$P < 0.01 relative to the Nob-treated group. $^{\&}$P < 0.05, $^{\&\&}$P < 0.01 relative to the tFNA-treated group.

2.6. The security of TNC in vivo

To verify the biocompatibility of TNC, we conducted experiments from two perspectives. First, we stained various organs and tissues (heart, liver, spleen, lung, and kidney) with HE stain. The results are shown in Fig. 7A. No significant changes were found, indicating that TNC is safe. Then, we conducted blood biochemical tests on each group of mice (Fig. 7B). The results also indicate that TNC is safe.

3. Conclusion

Oxidative stress and pyroptosis in chondrocytes, which lead to metabolic disorders in the ECM, are significant contributors to the pathogenesis and progression of OA. In this study, we successfully synthesized a novel DNA nanoparticle called TNC for OA treatment. The uptake of tFNA by chondrocytes is rapid and facile, enabling sustained release of Nob. Additionally, TNC exhibits excellent biocompatibility, biodegradability, and low cytotoxicity *in vivo*. Both *in vitro* and *in vivo* experiments have shown that Nob and tFNA can mitigate oxidative stress, cellular pyroptosis, and ECM catabolism associated with OA. Notably, TNC synergistically enhances the therapeutic effects both *in vitro* and *in vivo*. Therefore, we believe that TNC holds great clinical potential for treating OA.

4. Methods

4.1. Synthesis of tFNA and TNC

Initially, a mixture of four distinct single-stranded DNA oligonucleotides, as delineated in Table 1, was prepared in equimolar proportions from Shenggong Biotech (Shanghai, China.) This mixture was subsequently dissolved in a 1 × TM buffer solution, which was adjusted to a pH of 8.0 and contained Tris-HCl and magnesium chloride ($MgCl_2$). The solution underwent thermal denaturation by heating at 95 °C for 10 min, followed by controlled cooling to 4 °C over a duration of 20 min. Afterwards, the tFNA with a concentration of 1000 nmol/L was combined with an optimal concentration of Nob. The resulting mixture was agitated for 6 h to facilitate the formation of a stable complex [34,63]. Then, the residual Nob was removed by centrifugation through a 30 kDa ultrafiltration tube.

4.2. Characterization of the tFNA and TNC

To evaluate the integrity of the synthesized tFNA and the TNC, agarose gel electrophoresis (AGE) was employed as an analytical tool. For morphological analysis, the nanostructure and dimensions of TNC were examined and measured using transmission electron microscopy (TEM, Hitachi HT7800, Japan) and atomic force microscopy (AFM, Bruker Dimension Icon, Germany), respectively. Additionally, the encapsulation efficiency of TNC was quantitatively analyzed using a spectrophotometer (Shimadzu RF-5301PC, Japan). The absorbance of

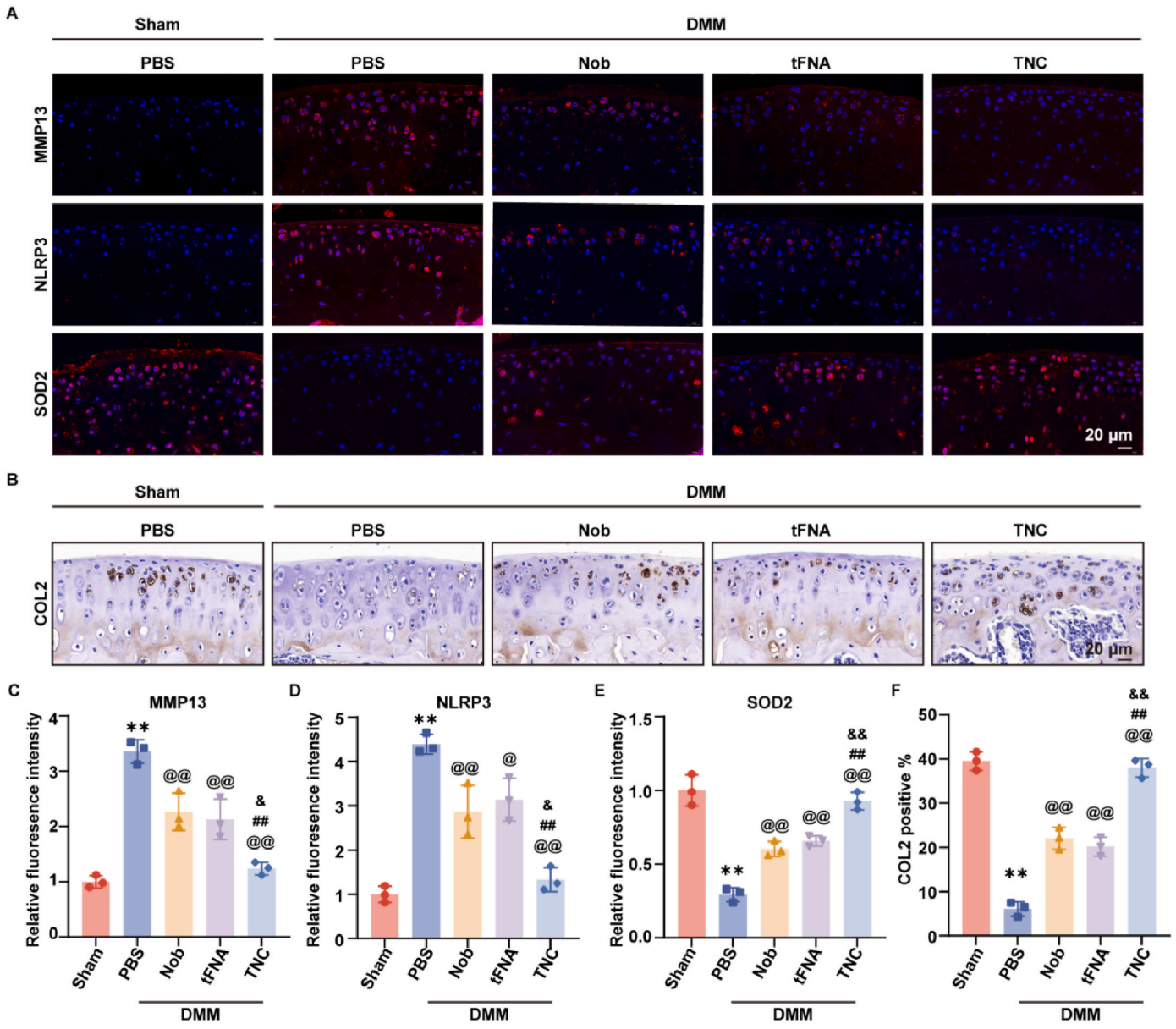

Fig. 6. (A) IF staining of MMP13, NLRP3, and SOD2 in mice knee joint articular cartilage under various treatment conditions at 8 weeks, n = 3. (B) Immunohistochemical staining of COL2 in mice knee joint articular cartilage under various treatment conditions at 8 weeks, n = 3. (C–E) Statistical analysis of IF staining of MMP13, NLRP3, and SOD2. (F) Statistical analysis of immunohistochemical staining of COL2. The data are presented as the mean ± SD. $^{*}p < 0.05$, $^{**}p < 0.01$ relative to the sham group. $^{@}P < 0.05$, $^{@@}P < 0.01$ relative to the DMM group. $^{\#}P < 0.05$, $^{\#\#}P < 0.01$ relative to the Nob-treated group. $^{\&}P < 0.05$, $^{\&\&}P < 0.01$ relative to the tFNA-treated group.

Nob at 340 nm wavelength was detected. The encapsulation and binding of Nob in TNC were further studied by spectral analysis. Equivalent TNC and Nob were dissolved in PBS (0.01 M, pH 7.4) to observe the solubility of the formulation [64].

Subsequently, the particle size distribution and zeta potential of both the tFNA and TNC were measured using a nanoparticle size analyzer (Malvern Zetasizer Nano ZS90, UK). To further investigate the *in vivo* stability of tFNA and TNC, they were incubated with fetal bovine serum (FBS) at varying concentrations (2 % or 10 %) and at multiple time points (0, 2, 4, 6, 8, 10, and 12 h), and their stability profiles were subsequently analyzed using AGE [37]. Finally, the distribution of tFNA and TNC within the gel was captured and documented using a gel imaging system (Bio-Rad Gel Doc XR, USA).

4.3. Cell culture

The human chondrocyte line C28/I2 was purchased from the Cell Bank of the Chinese Academy of Science (Shanghai, China). C28/I2 cells were cultured in Dulbecco's modified Eagle's medium (DMEM, Gibco, USA) supplemented with 10 % FBS (Gibco, USA) and 1 % penicillin/streptomycin (Gibco, USA) and maintained in an incubator at 37 °C with 5 % CO_2.

4.4. C28/I2 uptake by the TFNA and TNC

To confirm the successful uptake of TNC by C28/I2 cells, we initially labeled single-stranded nucleic acids with a Cy5 fluorescent molecule (Cy5-S1). Subsequently, C28/I2 cells were cocultured with Cy5-tFNA or Cy5-TNC at a concentration of 250 nM for 4 or 12h, respectively. After coculture, the cells were harvested and fixed with 4 %

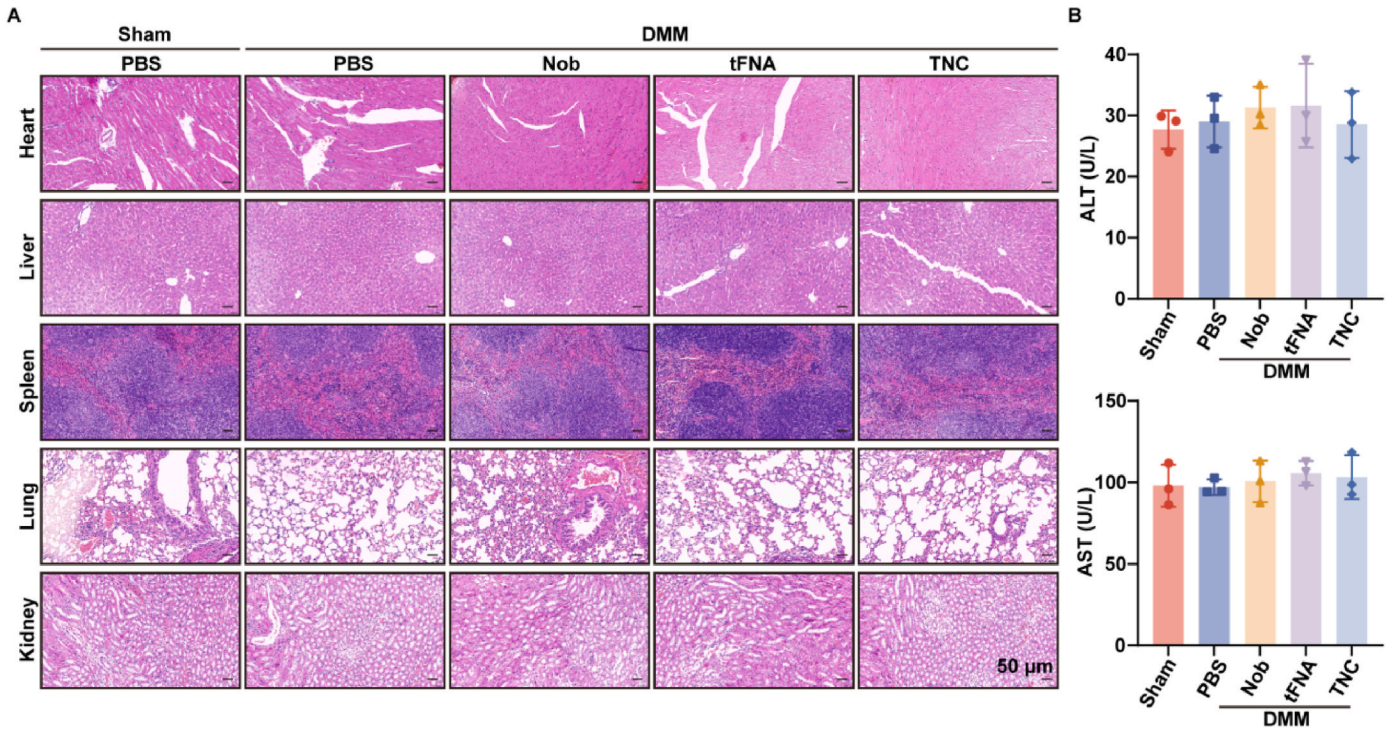

Fig. 7. ***In vivo*** **safety assessment of Nob, tFNA, and TNC. (A)** HE staining of important organs in mice for safety evaluation. (B) Blood biochemical examination in mice for safety evaluation.

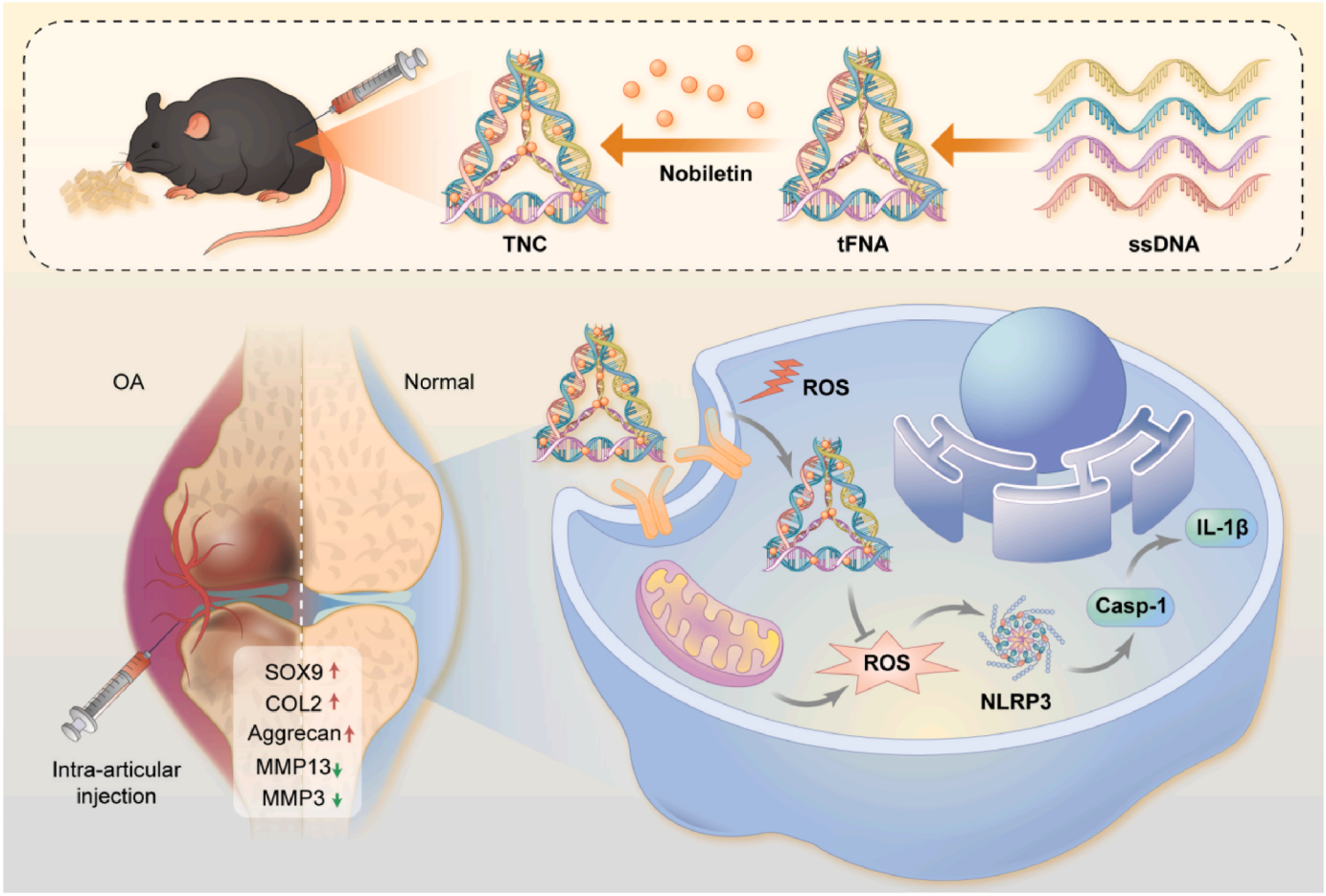

Fig. 8. The mechanistic illustration of TNC in alleviating oxidative stress and pyroptosis induced by TBHP in chondrocytes and in a DMM-induced OA mouse model.

paraformaldehyde (PFA) for 30 min. The C28/I2 cells were then stained with fluorescein isothiocyanate (FITC)-conjugated phalloidin (Beyotime, Shanghai, China) and 4′,6-diamidino-2-phenylindole (DAPI) (Beyotime, Shanghai, China) to observe the cytoskeleton and nucleus, respectively, of the cells.

4.5. ROS detection at the cellular level

In our study, we employed DCFH-DA (Beyotime, Shanghai, China) probe to assess the levels of ROS within cells and mitochondria, respectively. This approach allowed us to evaluate the oxidative stress status of cells. In brief, cells were first seeded in a 24-well plate and allowed to reach 50 % confluence before staining with DCFH-DA probes. After washing the cells with PBS (phosphate-buffered saline), the cells were subsequently incubated in serum-free medium at 37 °C supplemented with DCFH-DA (10 μM) for 30 min. Finally, the cells were observed under a fluorescence microscope, and the fluorescence intensity was quantified using ImageJ software.

4.6. Mitochondrial membrane potential measurement

We utilized JC-1 to assess the mitochondrial membrane potential. Briefly, the cells were incubated with the JC-1 probe for 30 min under light-protected conditions. Subsequently, the cells were washed three times with PBS, and finally, cellular observation was conducted using an Olympus FV3000 confocal microscope.

4.7. Evaluation of SOD and MDA

A malondialdehyde (MDA) assay kit (Beyotime, Shanghai, China) and total superoxide dismutase (SOD) assay kit (Beyotime, Shanghai, China) were used to measure the expression of SOD and MDA, respectively, as indicators of oxidative stress.

4.8. Live/dead cell staining

A Calcein/PI Cell Viability/Cytotoxicity Assay Kit (Beyotime, Shanghai, China) was used to detect cell viability. First, C28/I2 cells were inoculated into a 96-well plate, and once the cell density reached 70–80 % confluence, live/dead staining was performed. After washing three times with PBS, an appropriate volume of calcein AM/PI working solution was added for cell viability assessment. The cells were then incubated at 37 °C in the dark for 30 min. Ultimately, images were captured using a fluorescence microscope for analysis.

4.9. Alcian blue and toluidine blue staining

C28/I2 cells were plated in a 24-well plate and allowed to grow until they reached 80 % confluence for subsequent experimentation. The cells were then fixed with 4 % PFA for 30 min, followed by rinsing with PBS. Subsequently, the cells were stained with Alcian blue (Beyotime, Shanghai, China) and solution and toluidine blue (Sigma–Aldrich, USA) and incubated at 37 °C for 1 h.

4.10. Western blotting

After being washed three times with prechilled PBS, the cells were lysed by the addition of RIPA buffer (Beyotime, Shanghai, China), which is a strong lysis buffer supplemented with phosphatase inhibitors (Beyotime, Shanghai, China) and protease inhibitors (Beyotime, Shanghai, China). Subsequently, the protein concentration of the cell lysate was quantified using a BCA assay kit (Beyotime, Shanghai, China). Proteins were then diluted with 5× SDS–PAGE sample loading buffer and denatured at 95 °C for 8 min. Cellular proteins (20 μg) were subjected to electrophoresis on a 12 % sodium dodecyl sulfate polyacrylamide gel (SDS–PAGE) and transferred onto a polyvinylidene fluoride (PVDF) membrane. After blocking with 5 % bovine serum albumin (BSA), the membrane was incubated overnight at 4 °C with the following primary antibodies (each at a dilution of 1:1000): Caspase 1, SOX9, MMP13, MMP3, and β-actin (Proteintech, Wuhan, China); NLRP3 and IL-1β (Abcam, Cambridge, UK); and Collagen II (Affinity, USA). On the following day, based on the type of primary antibody corresponding to the secondary antibody, the PVDF membrane was incubated with HRP-conjugated IgG secondary antibody at room temperature for 1 h. Ultimately, the bands were visualized using an ECL Plus detection reagent kit, and the band intensities were quantified using ImageJ software.

4.11. Cellular IF staining

First, C28/I2 cells were inoculated into a 24-well plate, and once the cell density reached 70–80 % confluence, IF staining was performed. The cells were then fixed with 4 % PFA for 30 min, followed by rinsing with PBS. Subsequently, the cells were permeabilized with 0.5 % Triton X-100 for 30 min and then blocked with 0.5 % BSA for 20 min. Thereafter, the cells were incubated with the appropriate primary antibodies, followed by the application of secondary antibodies. Ultimately, the cells were examined under an Olympus FV3000 confocal microscope.

4.12. ELISA measurement

Using ELISA, we assessed the levels of TNF-α, IL-1β, IL-6 (Abcam, Cambridge, UK), and PGE2 (Cusabio, Wuhan, China) in the supernatants of C28/I2 cells, as well as the intracellular levels of 8-OHdG (Cusabio, Wuhan, China). The supernatants and cells were collected and subjected to the corresponding analyses according to the manufacturer's instructions.

4.13. DMM-induced OA mouse models

Compliance with ethical guidelines and protocols was maintained throughout all animal-based research, adhering to the principles outlined by the NIH. The study involving mice was approved by the Animal Experimentation Ethics Committee of Zhejiang University (reference number: ZJU20240332). Eight-week-old male C57BL/6 mice were housed individually and maintained under standardized conditions for the experiment. As previously described [65], the OA model was established using DMM surgery. The DMM was made as follows: the mice were first anesthetized with sodium pentobarbital, and the joint capsule was cut to expose the medial meniscus tibial ligament (MMTL). Then, the MMTL was cut, causing subluxation of the medial meniscus. For the sham group, the joint capsule of the mice was merely opened without any additional manipulation and was then directly sutured closed. 10 μL of PBS or varying formulations (tFNA, Nob, or TNC) was injected into the joint cavity daily after DMM. Following a consecutive 4-week and 8-week treatment period, the mice were euthanized, followed by subsequent testing.

4.14. Histological analysis and scoring system

The five organs and knee joints of the mice were fixed with 4 % PFA, followed by decalcification of the knee joints with EDTA. Thereafter, both the organs and knee joints were paraffin-embedded, and 5 μm sections were prepared. HE staining was applied to both the five organs and knee joints, while the knee joints were subjected to Alcian blue, Safranin O and Masson staining. The articular cartilage destruction in mice was assessed using the Osteoarthritis Research Society International (OARSI) scoring system for the medial tibial condyle.

4.15. Immunofluorescence and immunohistochemical staining in vivo

Initially, the paraffin-embedded sections were incubated at 60 °C for

1 h. Subsequently, the sections were deparaffinized in xylene and rehydrated through a graded series of alcohol solutions, each for 5 min, in the following sequence: xylene I, xylene II, anhydrous ethanol, 95 % ethanol I, 95 % ethanol II, 85 % ethanol, and 75 % ethanol. Endogenous peroxidase activity was then blocked with 3 % H_2O_2. Next, the sections were blocked with 10 % BSA before being incubated with the following primary antibodies overnight at 4 °C: MMP13 (diluted 1:100), NLRP3 (diluted 1:200), and SOD2 (diluted 1:200). Ultimately, the slides were incubated with Alexa Fluor-conjugated secondary antibodies and examined under an Olympus FV3000 confocal microscope. Standard protocols were used for IHC on paraffin sections. The following antibodies were applied: Collagen II (diluted 1:100). Then, the sections were stained with secondary antibodies and DAB substrate.

4.16. Statistical analysis

The results are expressed as the mean ± SD. One-way analysis of variance (ANOVA) or the Kruskal-Wallis test (for nonparametric data) was used to calculate statistical significance. All the statistical analyses were conducted using GraphPad Prism version 9.0 software. A P value < 0.05 was considered to indicate statistical significance.

CRediT authorship contribution statement

Jiafeng Li: Writing – original draft, Investigation, Conceptualization. **Yifan Li:** Writing – original draft, Visualization, Investigation. **Xiushuai Shang:** Writing – original draft, Methodology, Conceptualization. **Sheng Xu:** Visualization, Formal analysis. **Zhen Zhang:** Methodology. **Sanzhong Xu:** Writing – review & editing, Funding acquisition, Conceptualization. **Xuanwei Wang:** Writing – review & editing, Supervision, Data curation. **Miaoda Shen:** Writing – review & editing, Project administration, Conceptualization.

Declaration of competing interest

The authors declare that they have no known competing financial interests or personal relationships that could have appeared to influence the work reported in this paper.

Data availability

Data will be made available on request.

Acknowledgments

This work was supported by the National Natural Science Foundation of China (82172419). The authors would like to thank Home for Researcher for help in the preparation of Fig. 1A and 8 (www.home-for-researchers.com). The authors also thank Shiyanjia Lab (www.shiyanjia.com) for assisting with the AFM and TEM analyses.

Appendix A. Supplementary data

Supplementary data to this article can be found online at https://doi.org/10.1016/j.mtbio.2024.101202.

References

[1] J. Martel-Pelletier, A.J. Barr, F.M. Cicuttini, P.G. Conaghan, C. Cooper, M. B. Goldring, S.R. Goldring, G. Jones, A.J. Teichtahl, J.-P. Pelletier, Osteoarthritis, Nat. Rev. Dis. Prim. 2 (2016) 16072, https://doi.org/10.1038/nrdp.2016.72.

[2] S. Kwon, W. Kim, S. Yang, K.H. Choi, Influence of the type of occupation on osteoarthritis of the knee in men: the Korean national health and nutrition examination survey 2010-2012, J. Occup. Health 61 (2019) 54–62, https://doi.org/10.1002/1348-9585.12022.

[3] C. Lambert, J. Zappia, C. Sanchez, A. Florin, J.-E. Dubuc, Y. Henrotin, The damage-associated molecular patterns (DAMPs) as potential targets to treat osteoarthritis: perspectives from a review of the literature, Front. Med. 7 (2020) 607186, https://doi.org/10.3389/fmed.2020.607186.

[4] Q. Wang, A.L. Rozelle, C.M. Lepus, C.R. Scanzello, J.J. Song, D.M. Larsen, J. F. Crish, G. Bebek, S.Y. Ritter, T.M. Lindstrom, I. Hwang, H.H. Wong, L. Punzi, A. Encarnacion, M. Shamloo, S.B. Goodman, T. Wyss-Coray, S.R. Goldring, N. K. Banda, J.M. Thurman, R. Gobezie, M.K. Crow, V.M. Holers, D.M. Lee, W. H. Robinson, Identification of a central role for complement in osteoarthritis, Nat. Med. 17 (2011) 1674–1679, https://doi.org/10.1038/nm.2543.

[5] M.J. Alcaraz, M.I. Guillén, M.L. Ferrándiz, Emerging therapeutic agents in osteoarthritis, Biochem. Pharmacol. 165 (2019) 4–16, https://doi.org/10.1016/j.bcp.2019.02.034.

[6] X. Zhou, L. Jiang, G. Fan, H. Yang, L. Wu, Y. Huang, N. Xu, J. Li, Role of the ciRS-7/miR-7 axis in the regulation of proliferation, apoptosis and inflammation of chondrocytes induced by IL-1β, Int. Immunopharm. 71 (2019) 233–240, https://doi.org/10.1016/j.intimp.2019.03.037.

[7] M. Marullo, R.N. Tandogan, N. Kort, A. Meena, M. Attri, B. Gomberg, R. D'Ambrosi, Trends in unicompartmental knee arthroplasty among 138 international experienced arthroplasty knee surgeons, Heliyon 10 (2024) e24307, https://doi.org/10.1016/j.heliyon.2024.e24307.

[8] Y. Yu, H. Zheng, J.A. Buckwalter, J.A. Martin, Single cell sorting identifies progenitor cell population from full thickness bovine articular cartilage, Osteoarthritis Cartilage 22 (2014) 1318–1326, https://doi.org/10.1016/j.joca.2014.07.002.

[9] J. Lu, H. Zhang, D. Cai, C. Zeng, P. Lai, Y. Shao, H. Fang, D. Li, J. Ouyang, C. Zhao, D. Xie, B. Huang, J. Yang, Y. Jiang, X. Bai, Positive-feedback regulation of subchondral H-type vessel formation by chondrocyte promotes osteoarthritis development in mice, J. Bone Miner. Res. 33 (2018) 909–920, https://doi.org/10.1002/jbmr.3388.

[10] M.B. Goldring, S.R. Goldring, Articular cartilage and subchondral bone in the pathogenesis of osteoarthritis, Ann. N. Y. Acad. Sci. 1192 (2010) 230–237, https://doi.org/10.1111/j.1749-6632.2009.05240.x.

[11] M. Kapoor, J. Martel-Pelletier, D. Lajeunesse, J.-P. Pelletier, H. Fahmi, Role of proinflammatory cytokines in the pathophysiology of osteoarthritis, Nat. Rev. Rheumatol. 7 (2011) 33–42, https://doi.org/10.1038/nrrheum.2010.196.

[12] Z. Gong, J. Zhu, J. Chen, F. Feng, H. Zhang, Z. Zhang, C. Song, K. Liang, S. Yang, S. Fan, X. Fang, S. Shen, CircRREB1 mediates lipid metabolism related senescent phenotypes in chondrocytes through FASN post-translational modifications, Nat. Commun. 14 (2023) 5242, https://doi.org/10.1038/s41467-023-40975-7.

[13] J. Xie, J. Lin, M. Wei, Y. Teng, Q. He, G. Yang, X. Yang, Sustained Akt signaling in articular chondrocytes causes osteoarthritis via oxidative stress-induced senescence in mice, Bone Res 7 (2019) 23, https://doi.org/10.1038/s41413-019-0062-y.

[14] T. Ebata, M.A. Terkawi, K. Kitahara, S. Yokota, J. Shiota, Y. Nishida, G. Matsumae, H. Alhasan, M. Hamasaki, K. Hontani, T. Shimizu, D. Takahashi, T. Endo, T. Onodera, K. Kadoya, N. Iwasaki, Noncanonical pyroptosis triggered by <scp>Macrophage-Derived</scp> extracellular vesicles in chondrocytes leading to cartilage catabolism in osteoarthritis, Arthritis Rheumatol. 75 (2023) 1358–1369, https://doi.org/10.1002/art.42505.

[15] P. Lepetsos, K.A. Papavassiliou, A.G. Papavassiliou, Redox and NF-κB signaling in osteoarthritis, Free Radic. Biol. Med. 132 (2019) 90–100, https://doi.org/10.1016/j.freeradbiomed.2018.09.025.

[16] W. Hui, D.A. Young, A.D. Rowan, X. Xu, T.E. Cawston, C.J. Proctor, Oxidative changes and signalling pathways are pivotal in initiating age-related changes in articular cartilage, Ann. Rheum. Dis. 75 (2016) 449–458, https://doi.org/10.1136/annrheumdis-2014-206295.

[17] J.M. Abais, M. Xia, Y. Zhang, K.M. Boini, P.-L. Li, Redox regulation of NLRP3 inflammasomes: ROS as trigger or effector? Antioxidants Redox Signal. 22 (2015) 1111–1129, https://doi.org/10.1089/ars.2014.5994.

[18] Z. Luo, H. Zeng, K. Yang, Y. Wang, FOXQ1 inhibits the progression of osteoarthritis by regulating pyroptosis, Aging 16 (2024) 5077–5090, https://doi.org/10.18632/aging.205600.

[19] Y. Chen, D. Zeng, G. Wei, Z. Liao, R. Liang, X. Huang, W. Lu, Y. Chen, Pyroptosis in osteoarthritis: molecular mechanisms and therapeutic implications, JIR 17 (2024) 791–803, https://doi.org/10.2147/JIR.S445573.

[20] D. Wallach, T.-B. Kang, C.P. Dillon, D.R. Green, Programmed necrosis in inflammation: toward identification of the effector molecules, Science 352 (2016), https://doi.org/10.1126/science.aaf2154 aaf2154.

[21] S.M. Gregory, B.K. Davis, J.A. West, D.J. Taxman, S. Matsuzawa, J.C. Reed, J.P. Y. Ting, B. Damania, Discovery of a viral NLR homolog that inhibits the inflammasome, Science 331 (2011) 330–334, https://doi.org/10.1126/science.1199478.

[22] J. Shi, W. Gao, F. Shao, Pyroptosis: gasdermin-mediated programmed necrotic cell death, Trends Biochem. Sci. 42 (2017) 245–254, https://doi.org/10.1016/j.tibs.2016.10.004.

[23] Z. Huang, V.B. Kraus, Does lipopolysaccharide-mediated inflammation have a role in OA? Nat. Rev. Rheumatol. 12 (2016) 123–129, https://doi.org/10.1038/nrrheum.2015.158.

[24] A.R. Tall, M. Westerterp, Inflammasomes, neutrophil extracellular traps, and cholesterol, JLR (J. Lipid Res.) 60 (2019) 721–727, https://doi.org/10.1194/jlr.S091280.

[25] X. Chang, Y. Kang, Y. Yang, Y. Chen, Y. Shen, C. Jiang, Y. Shen, Pyroptosis: a novel intervention target in the progression of osteoarthritis, JIR 15 (2022) 3859–3871, https://doi.org/10.2147/JIR.S368501.

[26] C. Lou, Y. Fang, Y. Mei, W. Hu, L. Sun, C. Jin, H. Chen, W. Zheng, Cucurbitacin B attenuates osteoarthritis development by inhibiting <scp>NLRP3</scp> inflammasome activation and pyroptosis through activating <scp>Nrf2</scp>/

<scp>HO</scp>-1 pathway, Phytother Res. (2024), https://doi.org/10.1002/ptr.8209.

[27] G. Zhang, C. Huang, R. Wang, J. Guo, Y. Qin, S. Lv, Chondroprotective effects of Apolipoprotein D in knee osteoarthritis mice through the PI3K/AKT/mTOR signaling pathway, Int. Immunopharm. 133 (2024) 112005, https://doi.org/10.1016/j.intimp.2024.112005.

[28] W. Song, L. Zhang, X. Cui, R. Wang, J. Ma, Y. Xu, Y. Jin, D. Wang, Z. Lu, Nobiletin alleviates cisplatin-induced ototoxicity via activating autophagy and inhibiting NRF2/GPX4-mediated ferroptosis, Sci. Rep. 14 (2024) 7889, https://doi.org/10.1038/s41598-024-55614-4.

[29] M.M. El Tabaa, M.M. El Tabaa, R.M. Elgharabawy, W.G. Abdelhamid, Suppressing NLRP3 activation and PI3K/AKT/mTOR signaling ameliorates amiodarone-induced pulmonary fibrosis in rats: a possible protective role of nobiletin, Inflammopharmacol 31 (2023) 1373–1386, https://doi.org/10.1007/s10787-023-01168-2.

[30] Y. Hosokawa, I. Hosokawa, K. Ozaki, Nobiletin decreases inflammatory mediator expression in tumor necrosis factor-stimulated human periodontal ligament cells, Mediat. Inflamm. 2021 (2021) 1–7, https://doi.org/10.1155/2021/5535844.

[31] W. Chai, J. Zhang, Z. Xiang, H. Zhang, Z. Mei, H. Nie, R. Xu, P. Zhang, Potential of nobiletin against Alzheimer's disease through inhibiting neuroinflammation, Metab. Brain Dis. 37 (2022) 1145–1154, https://doi.org/10.1007/s11011-022-00932-7.

[32] L. Xie, H. Xie, C. Chen, Z. Tao, C. Zhang, L. Cai, Inhibiting the PI3K/AKT/NF-κB signal pathway with nobiletin for attenuating the development of osteoarthritis:*in vitro*and*in vivo*studies, Food Funct. 10 (2019) 2161–2175, https://doi.org/10.1039/C8FO01786G.

[33] Z. Liu, S. Guo, Q. Dong, Nobiletin suppresses IL-21/IL-21 receptor-mediated inflammatory response in MH7A fibroblast-like synoviocytes (FLS): an implication in rheumatoid arthritis, Food Funct. 10 (2020) 172939, https://doi.org/10.1016/j.ejphar.2020.172939.

[34] T. Tian, T. Zhang, S. Shi, Y. Gao, X. Cai, Y. Lin, A dynamic DNA tetrahedron framework for active targeting, Nat. Protoc. 18 (2023) 1028–1055, https://doi.org/10.1038/s41596-022-00791-7.

[35] S. Shi, Y. Chen, T. Tian, S. Li, S. Lin, Y. Zhang, X. Shao, T. Zhang, Y. Lin, X. Cai, Effects of tetrahedral framework nucleic acid/wogonin complexes on osteoarthritis, Bone Res 8 (2020), https://doi.org/10.1038/s41413-019-0077-4.

[36] J. Li, Y. Yao, Y. Wang, J. Xu, D. Zhao, M. Liu, S. Shi, Y. Lin, Modulation of the crosstalk between schwann cells and macrophages for nerve regeneration: a therapeutic strategy based on a multifunctional tetrahedral framework nucleic acids system, Adv. Mater. 34 (2022) e2202513, https://doi.org/10.1002/adma.202202513.

[37] Y. Li, Z. Cai, W. Ma, L. Bai, E. Luo, Y. Lin, A DNA tetrahedron-based ferroptosis-suppressing nanoparticle: superior delivery of curcumin and alleviation of diabetic osteoporosis, Bone Res 12 (2024), https://doi.org/10.1038/s41413-024-00319-7.

[38] Y. Chen, X. Chen, B. Zhang, Y. Zhang, S. Li, Z. Liu, Y. Gao, Y. Zhao, L. Yan, Y. Li, T. Tian, Y. Lin, DNA framework signal amplification platform-based high-throughput systemic immune monitoring, Signal Transduct. Targeted Ther. 9 (2024) 1–17, https://doi.org/10.1038/s41392-024-01736-0.

[39] S. Shi, T. Tian, Y. Li, D. Xiao, T. Zhang, P. Gong, Y. Lin, Tetrahedral framework nucleic acid inhibits chondrocyte apoptosis and oxidative stress through activation of autophagy, ACS Appl. Mater. Interfaces 12 (2020) 56782–56791, https://doi.org/10.1021/acsami.0c17307.

[40] Y. Zhao, S. Li, M. Feng, M. Zhang, Z. Liu, Y. Yao, T. Zhang, Y. Jiang, Y. Lin, X. Cai, Effects of puerarin-loaded tetrahedral framework nucleic acids on osteonecrosis of the femoral head, Small 19 (2023), https://doi.org/10.1002/smll.202302326.

[41] M. Zhang, X. Zhang, T. Tian, Q. Zhang, Y. Wen, J. Zhu, D. Xiao, W. Cui, Y. Lin, Anti-inflammatory activity of curcumin-loaded tetrahedral framework nucleic acids on acute gouty arthritis, Bioact. Mater. 8 (2022) 368–380, https://doi.org/10.1016/j.bioactmat.2021.06.003.

[42] Y. Li, J. Li, S. Xu, D. Li, Z. Zhang, Q. Huang, X. Wang, M. Shen, S. Xu, Tetrahedral framework nucleic acid-based delivery of astaxanthin suppresses chondrocyte pyroptosis and modulates oxidative stress for the treatment of osteoarthritis, Adv Healthcare Materials n/a (2024) 2401452, https://doi.org/10.1002/adhm.202401452.

[43] Y. Wen, M. Zhang, Y. Yao, Y. Gao, X. Zhang, Y. Lin, X. Cai, Biological regulation on synovial fibroblast and the treatment of rheumatoid arthritis by nobiletin-loaded tetrahedral framework nucleic acids cargo tank, Chin. Chem. Lett. 34 (2023) 107549, https://doi.org/10.1016/j.cclet.2022.05.063.

[44] S. Shi, T. Chen, W. Lu, Y. Chen, D. Xiao, Y. Lin, Amelioration of osteoarthritis via tetrahedral framework nucleic acids delivering microrna-124 for cartilage regeneration, Adv. Funct. Mater. 33 (2023) 2305558, https://doi.org/10.1002/adfm.202305558.

[45] B. Qu, X. Wang, D. Zheng, C. Mai, Z. Liu, H. Zhou, Y. Xie, Novel treatment for refractory rheumatoid arthritis with total glucosides of paeony and nobiletin codelivered in a self-nanoemulsifying drug delivery system, Acta Pharmacol. Sin. 43 (2022) 2094–2108, https://doi.org/10.1038/s41401-021-00801-6.

[46] J. Ning, G. Zheng, Y. Cai, Y. Hu, Y. Liu, E. Lai, B. Chen, Y. Liu, Z. Liang, J. Fu, M. Wei, The self-assembly Soluplus nanomicelles of nobiletin in aqueous medium based on solid dispersion and their increased hepatoprotective effect on APAP-induced acute liver injury, IJN 18 (2023) 5119–5140, https://doi.org/10.2147/IJN.S426703.

[47] D. Wu, B. Zhou, J. Li, X. Wang, B. Li, H. Liang, Coordination-driven metal-polyphenolic nanoparticles toward effective anticancer therapy, Adv. Healthcare Mater. 11 (2022) 2200559, https://doi.org/10.1002/adhm.202200559.

[48] Y. Wang, J. Xie, Z. Ai, J. Su, p>Nobiletin-loaded micelles reduce ovariectomy-induced bone loss by suppressing osteoclastogenesis&lt, IJN 14 (2019) 7839–7849, https://doi.org/10.2147/IJN.S213724.

[49] Y.J. Kim, J. Han, S. Han, The interplay between endoplasmic reticulum stress and oxidative stress in chondrocyte catabolism, CARTILAGE (2024), https://doi.org/10.1177/19476035241245803, 19476035241245803.

[50] Z. Liu, X. Chen, W. Ma, Y. Gao, Y. Yao, J. Li, T. Zhang, X. Qin, Y. Ge, Y. Jiang, Y. Lin, Suppression of lipopolysaccharide-induced sepsis by tetrahedral framework nucleic acid loaded with quercetin, Adv. Funct. Mater. 32 (2022), https://doi.org/10.1002/adfm.202204587.

[51] H. Bai, Z. Zhang, L. Liu, X. Wang, X. Song, L. Gao, Activation of adenosine <scp>A3</scp> receptor attenuates progression of osteoarthritis through inhibiting the <scp>NLRP3</scp>/caspase-1/<scp>GSDMD</scp> induced signalling, J. Cell Mol. Med. 26 (2022) 4230–4243, https://doi.org/10.1111/jcmm.17438.

[52] G. Liu, Q. Liu, B. Yan, Z. Zhu, Y. Xu, USP7 inhibition alleviates H2O2-induced injury in chondrocytes via inhibiting NOX4/NLRP3 pathway, Front. Pharmacol. 11 (2023), https://doi.org/10.3389/fphar.2020.617270.

[53] J. Li, Y. Li, X. Wang, Y. Xie, J. Lou, Y. Yang, S. Jiang, M. Ye, H. Chen, W. Diao, S. Xu, Pinocembrin alleviates pyroptosis and apoptosis through <scp>ROS</scp> elimination in random skin flaps via activation of <scp>SIRT3</scp&gt, Phytother Res. 37 (2023) 4059–4075, https://doi.org/10.1002/ptr.7864.

[54] C. Dai, L. He, B. Ma, T. Chen, Facile nanolization strategy for therapeutic *ganoderma lucidum spore oil* to achieve enhanced protection against radiation-induced heart disease, Small 15 (2019) e1902642, https://doi.org/10.1002/smll.201902642.

[55] J. Zhou, J. Wu, F. Fu, S. Yao, W. Zheng, W. Du, H. Luo, H. Jin, P. Tong, C. Wu, H. Ruan, α-Solanine attenuates chondrocyte pyroptosis to improve osteoarthritis via suppressing <scp>NF-κB</scp> pathway, J. Cell Mol. Med. 28 (2024) e18132, https://doi.org/10.1111/jcmm.18132.

[56] J. Sui, F. Dai, J. Shi, C. Zhou, Ubiquitin-specific peptidase 25 exacerbated osteoarthritis progression through facilitating TXNIP ubiquitination and NLRP3 inflammasome activation, J. Orthop. Surg. Res. 18 (2023) 762, https://doi.org/10.1186/s13018-023-04083-y.

[57] H. Tang, X. Gong, J. Dai, J. Gu, Z. Dong, Y. Xu, Z. Hu, C. Zhao, J. Deng, S. Dong, The IRF1/GBP5 axis promotes osteoarthritis progression by activating chondrocyte pyroptosis, Journal of Orthopaedic Translation 44 (2024) 47–59, https://doi.org/10.1016/j.jot.2023.11.005.

[58] X. Chen, J. He, Y. Xie, T. Zhang, S. Li, Y. Zhao, N. Hu, X. Cai, Tetrahedral framework nucleic acid nanomaterials reduce the inflammatory damage in sepsis by inhibiting pyroptosis, Cell Prolif. 56 (2023) e13424, https://doi.org/10.1111/cpr.13424.

[59] Y. Jiang, S. Li, R. Shi, W. Yin, W. Lv, T. Tian, Y. Lin, A novel bioswitchable miRNA mimic delivery system: therapeutic strategies upgraded from tetrahedral framework nucleic acid system for fibrotic disease treatment and pyroptosis pathway inhibition, Adv. Sci. 11 (2024) e2305622, https://doi.org/10.1002/advs.202305622.

[60] M. Kapoor, J. Martel-Pelletier, D. Lajeunesse, J.-P. Pelletier, H. Fahmi, Role of proinflammatory cytokines in the pathophysiology of osteoarthritis, Nat. Rev. Rheumatol. 7 (2011) 33–42, https://doi.org/10.1038/nrrheum.2010.196.

[61] K. Imada, N. Lin, C. Liu, A. Lu, W. Chen, M. Yano, T. Sato, A. Ito, Nobiletin, a citrus polymethoxy flavonoid, suppresses gene expression and production of aggrecanases-1 and -2 in collagen-induced arthritic mice, Eur. J. Pharmacol. 373 (2008) 181–185, https://doi.org/10.1016/j.bbrc.2008.05.171.

[62] S. Shi, T. Tian, Y. Li, D. Xiao, T. Zhang, P. Gong, Y. Lin, Tetrahedral framework nucleic acid inhibits chondrocyte apoptosis and oxidative stress through activation of autophagy, ACS Appl. Mater. Interfaces 12 (2020) 56782–56791, https://doi.org/10.1021/acsami.0c17307.

[63] T. Zhang, T. Tian, R. Zhou, S. Li, W. Ma, Y. Zhang, N. Liu, S. Shi, Q. Li, X. Xie, Y. Ge, M. Liu, Q. Zhang, S. Lin, X. Cai, Y. Lin, Design, fabrication and applications of tetrahedral DNA nanostructure-based multifunctional complexes in drug delivery and biomedical treatment, Nat. Protoc. 15 (2020) 2728–2757, https://doi.org/10.1038/s41596-020-0355-z.

[64] M. Zhang, X. Zhang, T. Tian, Q. Zhang, Y. Wen, J. Zhu, D. Xiao, W. Cui, Y. Lin, Anti-inflammatory activity of curcumin-loaded tetrahedral framework nucleic acids on acute gouty arthritis, Bioact. Mater. 8 (2022) 368–380, https://doi.org/10.1016/j.bioactmat.2021.06.003.

[65] S.S. Glasson, T.J. Blanchet, E.A. Morris, The surgical destabilization of the medial meniscus (DMM) model of osteoarthritis in the 129/SvEv mouse, Osteoarthritis Cartilage 15 (2007) 1061–1069, https://doi.org/10.1016/j.joca.2007.03.006.